CCFE
CULHAM CENTRE FOR FUSION ENERGY

UK Atomic Energy Authority

UKAEA-CCFE-PR(21)74

Andrej Horvat, Mike Fursdon, Nicolas Mantel, Rob Bamber, Martin Webb, Davide Kleiner, Roberta Santori

# Thermal design of ITER ICH antenna straps

# Thermal design of ITER ICH antenna straps

Andrej Horvat, Mike Fursdon, Nicolas Mantel, Rob Bamber,
Martin Webb, Davide Kleiner, Roberta Santori

This is a preprint of a paper submitted for publication in
Fusion Engineering and Design

# Thermal design of ITER ICH antenna straps

Andrej Horvat[1]

Mike Fursdon, Nicolas Mantel, Rob Bamber, Martin Webb (Culham Centre for Fusion Energy)

Davide Kleiner, Roberta Santori (Fusion for Energy)

## Abstract

An important contribution to the mechanical stresses present in the ITER ICH antenna is related to the non-uniform heating of its front section due to RF losses, plasma and charge exchange, and the effects of neutron radiation. As a consequence, intensive convective cooling is necessary to maintain temperature and the related thermally induced stresses below their permissible levels.

Design effort had been focused on thermal design development of the ITER ICH antenna straps with the main objective to maximise cooling performance of their internal water channels. In the initial stage, a set of strap design variations was analysed using a representative 2D strap section to quantify thermal resistances associated with strap design elements, improve conductive heat transfer between load surfaces and coolant flow, enhance convective cooling, reduce mechanical stress in the straps, and to propose a strap design solution for a 3D thermo-structural analysis. As a result, the number of cooling channels was increased, and their diameter reduced. Although, reducing the strap thickness may also improve its thermal performance, disruption induced mechanical loading prohibits such a design solution. Different material combinations were evaluated to provide an acceptable compromise between the strap thermal performance, stiffness and allowable stress limits. Copper was removed from the design to reduce the electro-magnetic forces induced during disruptions and stainless steel 316L(N) was replaced with Inconel 625 to raise the allowable stress limits especially at elevated temperatures.

The thermal load contributions were reviewed due to significant uncertainties in their definition. Although minimal modifications were introduced in the assessment of thermal loads related to RF losses and neutron absorption, the thermal loads related to plasma and charge exchange were re-evaluated by performing Monte Carlo simulations of radiative heat transfer. This allowed for a more accurate approximation of the shielding effect from the antenna's Faraday screen and reduction of plasma related thermal loading.

For the developed ITER ICH antenna strap design, a 3D thermo-structural analysis was performed to assess its structural performance under the anticipated normal operating conditions where the thermal loading yields dominant stress contributions. The presented results exhibit significantly lower stresses than in the previous strap design and demonstrate compliance with the SDC-IC design criteria. Note that further development of the 4-port junction and the strap housing design has progressed since this work was concluded.

**Keywords:** ITER, ICH antenna, normal operating conditions, thermal loading, structural design, plasma and charge exchange, convective cooling, neutron heating

[1] Corresponding author (andrej.horvat@ukaea.uk)

## Introduction

The Ion Cyclotron Heating and Current Drive system antenna (IC H&CD, or in short, ICH antenna) will provide radiofrequency (RF) heating and current drive to ITER plasmas to assist in accessing the H-mode and achieving Q = 10. The heating power will also assist in accomplishing several functions of plasma control, such as control of plasma burn and transport. These functions will be met by delivering a nominal power of 20 MW to ITER plasmas in the frequency range of 40 to 55MHz by ICH antenna arrays incorporated in equatorial port plugs.

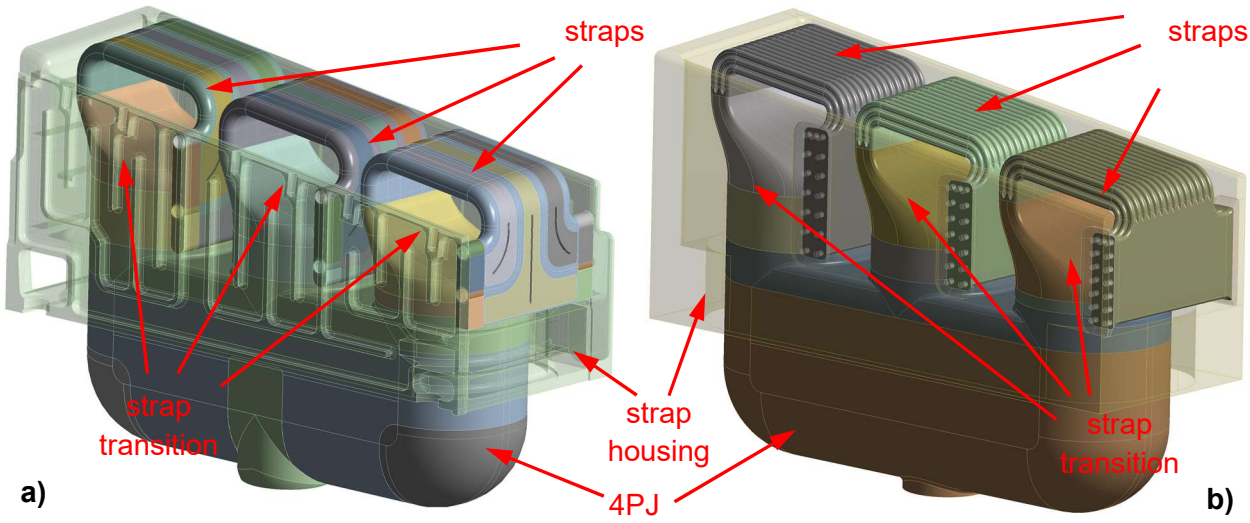


**Figure 1:** Front sections of the ICRH antenna - PDR design (a), proposed v12a design (b)

The front part of the ICH antenna and especially its straps (Fig. 1) are subjected to non-uniform heating due to RF losses, plasma and charge exchange, and the effects neutron radiation. Their thermal expansion is restricted by the 4-port junction (4PJ) body and the strap housing, which results in both bending and twisting of the cooling channels and straps.

Therefore, intensive convective cooling is necessary to maintain the temperature below its permissible level, in order to reduce thermally induced stresses. The approximate flow path of the cooling water is shown in Fig. 2. Previous design developments and associated analyses [1-2] have shown that maintaining operability and structural integrity even during normal operating conditions (NOC) remains a challenge.

In the current study, the effort had been focused on thermal design development of ITER ICH antenna straps with the main objective to maximise cooling performance of their internal water channels while retaining component manufacturability.

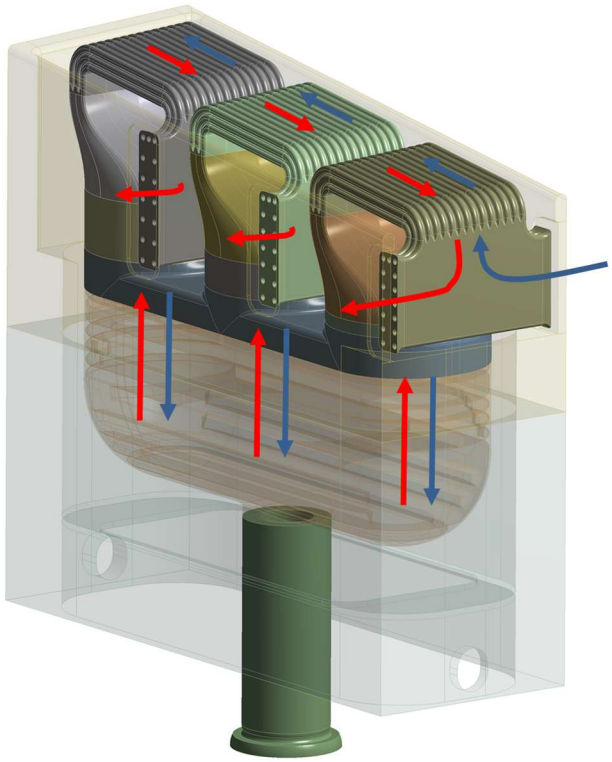

**Figure 2:**
Approximate flow path of the cooling water

## Optimisation of convective cooling

In the initial stage, a set of strap design variations was analysed using a representative 2D strap section to:

- quantify the thermal resistances associated with strap design elements,
- improve conductive heat transfer between load surfaces and coolant flow,
- enhance convective cooling,
- reduce mechanical stress in the straps,
- propose a strap design solution for a 3D thermo-structural analysis.

All together 32 strap design variations were examined to identify a strap design that can satisfy the design objectives. Thermo-structural FE models were prepared using a 2D slice of strap design variations to minimize the simulation time.

The heat loading that was defined for the Preliminary Design Review (PDR) [3] was also used for the initial 2D analysis. The FE models included surface heat fluxes due to plasma and RF loads, and the convective cooling associated with the Primary Heat Transfer System (PHTS) water flow. Figure 3 shows the applied surface heat fluxes as they were defined for the PDR [3]. However, no volumetric heating arising from neutron absorption was included at this stage primarily due to 3D nature of the load field.

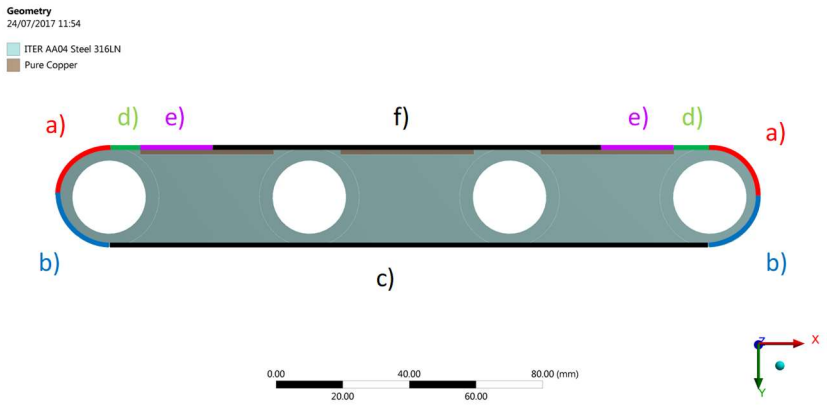


**Figure 3:** Strap heat flux distribution

**a)** 245 kW/m², **b)** 125 kW/m², **c)** 29 kW/m², **d)** 130 kW/m², **e)** 160 kW/m², **f)** 155 kW/m²

For the cooling channels, the convective heat transfer coefficient ($\alpha$) was calculated for the available total coolant mass flow rate of 3 kg/s. The Dittus-Boelter correlation for pipe flow was used to obtain the Nusselt number and hence estimate the heat transfer coefficient:

$$Nu = 0.023 Re_D^{0.8} Pr^{0.4} \quad \text{and} \quad \alpha = Nu \frac{k}{D} \tag{1}$$

The heat transfer coefficient was further increased by 13.4% to match the value obtained with 3D CFD analysis of the PDR strap design that was also performed.

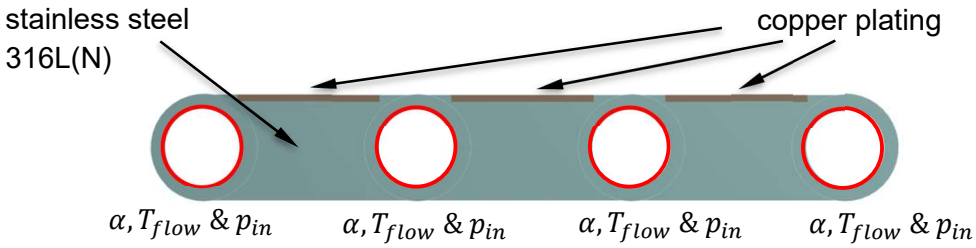


**Figure 4:** Example of strap convective heat transfer and pressure boundaries

The medium flow temperature of 83.5°C that was used in the convective heat transfer calculations was derived from the cooling water inlet temperature and the strap total energy balance. In addition to thermal loading, a pressure load of 5 MPa was assigned to the channel internal surfaces as shown in Fig. 4.

Figure 5 shows the temperature and the equivalent (von Mises) stress field for the PDR strap design. As its thermal and structural behaviour is symmetric, only half of the cross-section is presented. These results were used as a reference from which any design improvements were assessed.

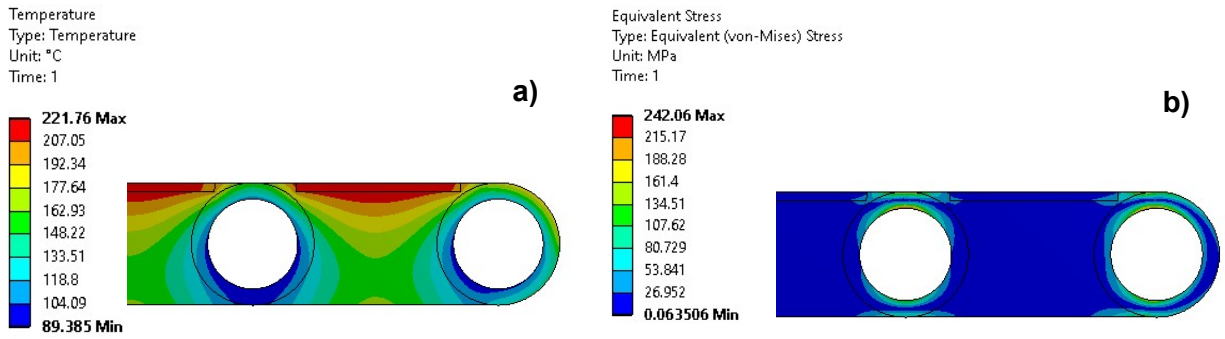


**Figure 5:** PDR strap design - temperature (a), and equivalent stress (b)

The assessment of thermal conditions and the resulting design optimisation led to an increase in the number of cooling channels and a reduction in their diameter. Figure 6 shows the temperature and the equivalent (von Mises) stress field for the proposed v12a strap design, which contains 28 cooling channels with an internal diameter of 9 mm. The channel wall thickness was decreased to 1 mm.

Although, reducing the strap thickness may also improve its thermal performance, the mechanical loading due to electro-magnetic (EM) disruption events prohibits such a design solution. For the same reason, copper plating was also removed from the strap design. In addition to this, material was removed between the channels to further reduce thermal resistance between the load surfaces and the coolant flow.

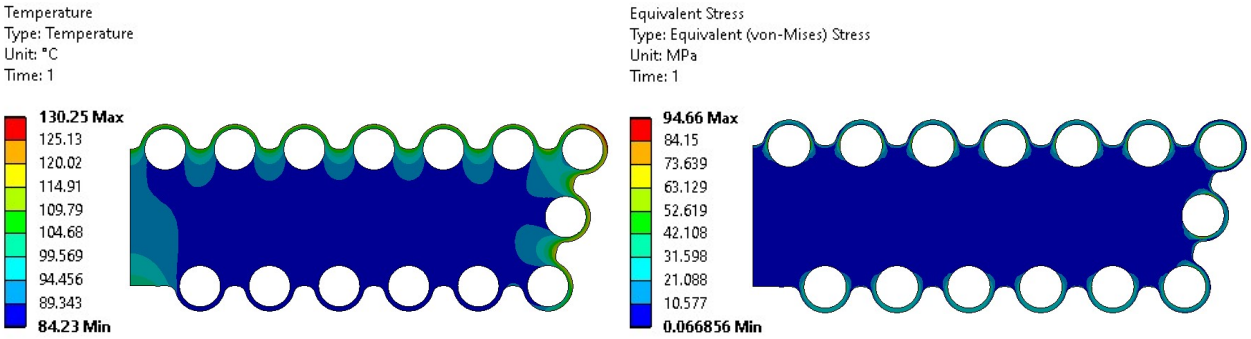


**Figure 6:** Proposed v12a design - temperature (a), and equivalent stress (b)

Results in Fig. 6 reveal a significant reduction in the maximum strap temperature and the associated stresses. Table 1 summarises the main design and operational parameters as well as achieved performance improvements for the strap design. Note only a small change in the flow speed between both designs.

**Table 1:** Main design and performance parameters for the PDR and the proposed v12a strap design

| | no of channels | channel inner diameter | flow speed |
|---|---|---|---|
| **PDR design** | 4 | 22 mm | 1.36 m/s |
| **proposed v12a design** | 28 | 9 mm | 1.12 m/s |

| | max temperature | max temperature difference | max equivalent stress |
|---|---|---|---|
| **PDR design** | 222°C | 138°C | 242 MPa |
| **proposed v12a design** | 130°C | 47°C | 95 MPa |

## Revision of thermal loading

For the 3D analysis, the original PDR heat loading was reviewed and then revised for improved accuracy. Although minimal modifications were introduced in the assessment of thermal loads related to RF losses and neutron absorption, the thermal loads related to plasma and charge exchange were re-evaluated by performing Monte Carlo simulations of radiative heat transfer.

The maximum load on the front face of 0.35 MW/m$^2$ [4] was taken into consideration. The shielding effect of the Faraday screen was assessed by using a Monte Carlo radiation solver in ANSYS CFX. Figure 7 shows a geometrical arrangement of the simulation domain, which covers a 2D representative section of the space between the Faraday screen and the straps.

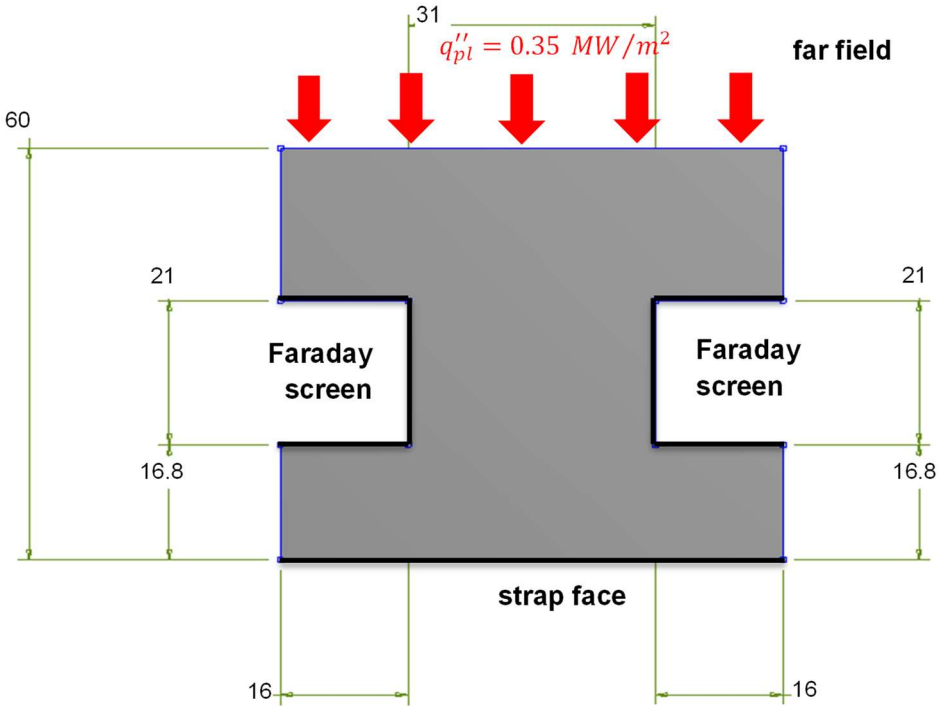


**Figure 7:** Simulation domain for the shielding effect analysis (all units are in millimetres)

The emissivity of the Faraday screen surfaces as well as that of the strap face was assumed to be 1.0. It must be noted that such assumption may not lead to conservative results as some reflection and local emission do occur.

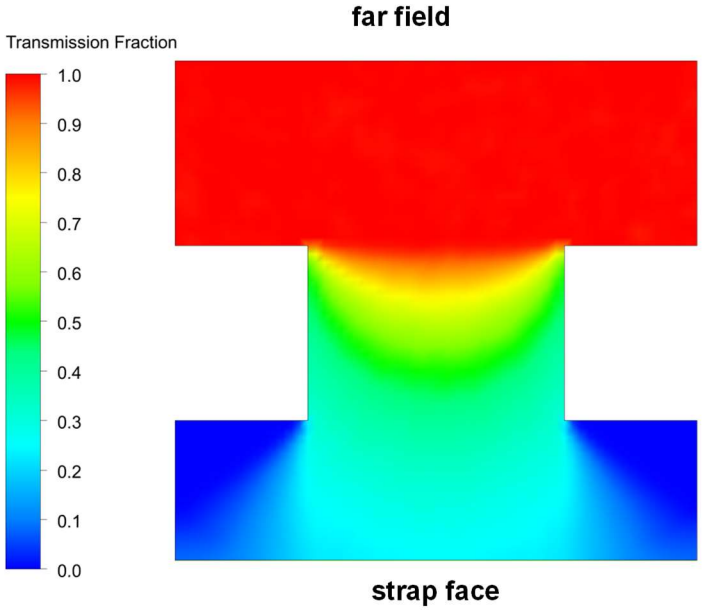


**Figure 8:** Transmissivity of the plasma and charge exchange related heat flux

Based on the calculated radiation intensity ($I$), the radiation transmissivity was defined as

$$\varepsilon_{trans} = \frac{2\pi I}{q''_{pl}} \tag{2}$$

where

$I$ is the calculated radiation intensity

$q''_{pl}$ is the far field irradiation heat flux related to plasma and charge exchange

Figure 8 shows the calculated transmissivity field. The overall Faraday screen transmissivity is simply an average value along the strap face, which was calculated to be 18.3%. Thermal loading onto strap faces due to plasma and charge exchange is then

$$q''_{pl}\big|_{strap\ face} = \bar{\varepsilon}_{trans}\, q''_{pl} \tag{3}$$

The variables in Eq. (3) represent surface averaged values with the maximum transmissivity being 41% higher than the average ($\bar{\varepsilon}_{trans}$).

The described Monte Carlo simulation method allowed more accurate approximation of shielding effect from the antenna's Faraday screen than that used in the PDR assessment. As a consequence, significantly reduced plasma related thermal loading was assigned to the ICH antenna straps in the FE model.

Figure 9 presents the overall surface heat loading that was assigned to the frontal sections of the ICH antenna. It includes the plasma and charge exchange related heat flux as well as thermal loading related to the RF losses.

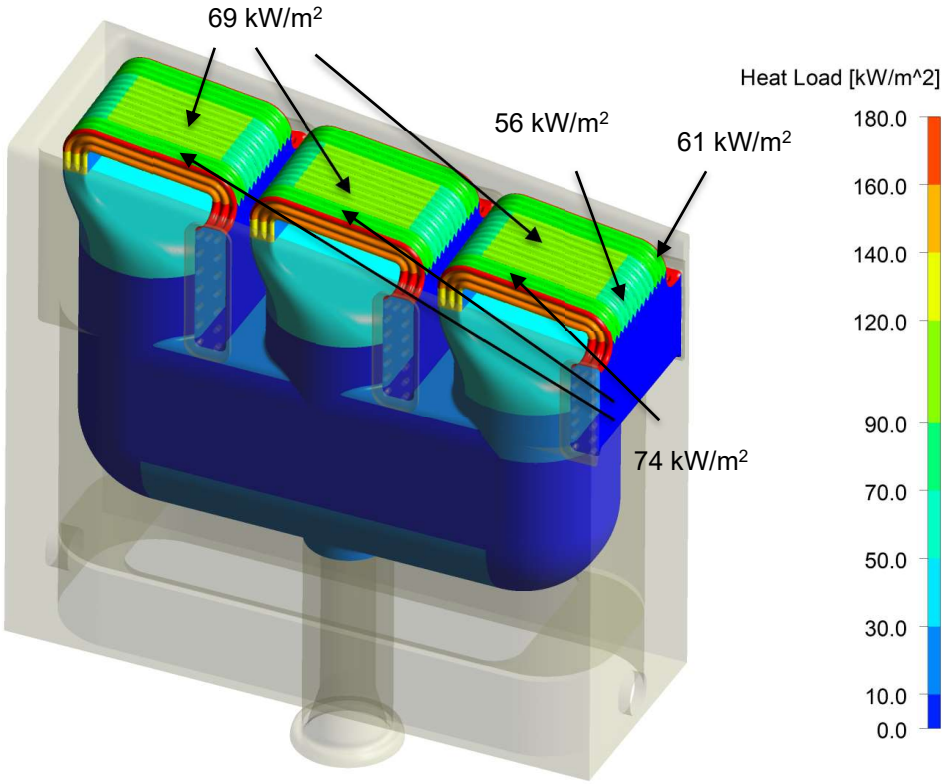


**Figure 9:** Prescribed heat flux to the frontal sections of the ICH antenna - proposed v12a design

Volumetric heating in the ICH antenna is associated with neutron radiation. The current load data are based on the B-lite reference model [5] with only a few manual alterations. The corresponding volumetric power density $q_i'''$ is presented in Table 2. Note that these values do change with the design although such variations are relatively small.

**Table 2:** Total heat load from volumetric sources for the proposed v12a design

| | Volume [$m^3$] | Power [W] | Power density [$W/m^3$] |
|---|---|---|---|
| **Straps** | 1.205E-02 | 2.763E+04 | 2.294E+06 |
| **Strap transition** | 1.027E-02 | 1.574E+04 | 1.532E+06 |
| **4PJ** | 1.991E-02 | 1.050E+04 | 5.272E+05 |
| **Total** | **4.223E-02** | **5.387E+04** | |

## Material considerations

Different material combinations were evaluated to provide an acceptable compromise between the strap thermal performance, stiffness and allowable stress limits. Although the analysis undertaken demonstrated that the increased extent of the copper plating helps in redistribution of high heat fluxes, copper was removed from the design to reduce the induced EM disruption forces. Also, stainless steel 316L(N) was replaced with Inconel 625 [8] to raise the allowable stress limits especially at elevated temperatures.

Structural evaluation of the PDR design and the proposed v12a design was conducted by applying Structural Design Criteria for ITER In-vessel Components (SDC-IC) [6]. Table 3 shows the allowable stress limits for the immediate plastic collapse and plastic instability ($S_m$), and the time-independent fatigue ($S_a$). The latter requirement considers 30,000 NOC and 830 category II events and allows for 50% usage for each load case [7].

**Table 3:** Allowable stress limits for stainless steel 316L(N) and Inconel 625 [8]

| | | stainless steel 316L(N) | Inconel 625 |
|---|---|---|---|
| **Immediate plastic collapse and plastic instability limit** | $S_m$ | 141 MPa @ 150°C | 258 MPa @ 150°C |
| **Time-independent fatigue limit** | $S_a$ | 434 MPa | 640 MPa |

## Design assessment and discussion

A three-dimensional thermo-structural FE analysis was performed to assess the structural performance of the proposed v12a strap design under anticipated normal operating conditions (NOC) where thermal loads cause dominant stress contributions.

Figures 10 and 11 show the temperature distribution in the frontal part of the PDR and the proposed v12a design, respectively. The maximum temperature in the proposed v12a design is approximately 100°C lower than in the PDR design. Such a large temperature decrease is mostly attributed to the reduction of cooling channel wall thickness and therefore to the substantial improvement of heat conduction between the loading surfaces and the cooling water.

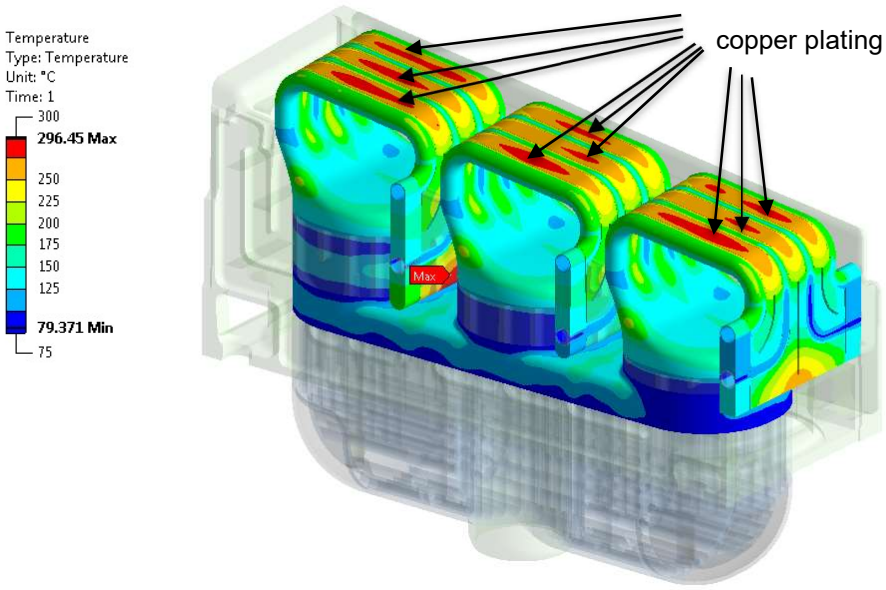


**Figure 10:** Temperature in the frontal sections of the ICH antenna - PDR design

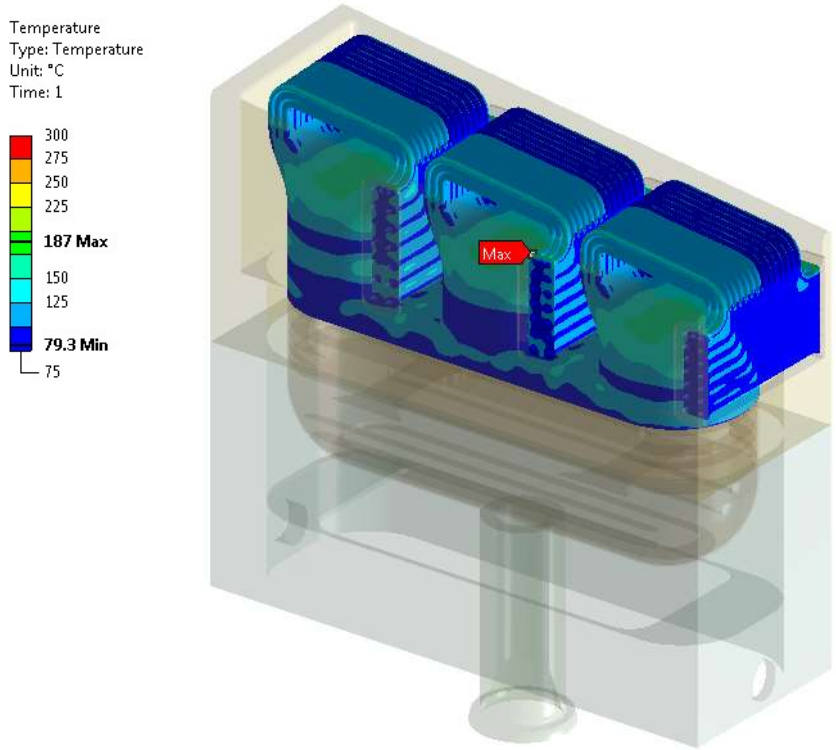


**Figure 11:** Temperature in the frontal sections of the ICH antenna - proposed v12a design

Elastic structural modelling was used exclusively for all the FE analyses performed. Figure 12 presents stress intensities for the initial PDR design. Although the maximum stress of 1143 MPa

can be attributed to a local stress concentration (Fig. 13), wider areas do exceed the allowable stress limit for stainless steel 316L(N).

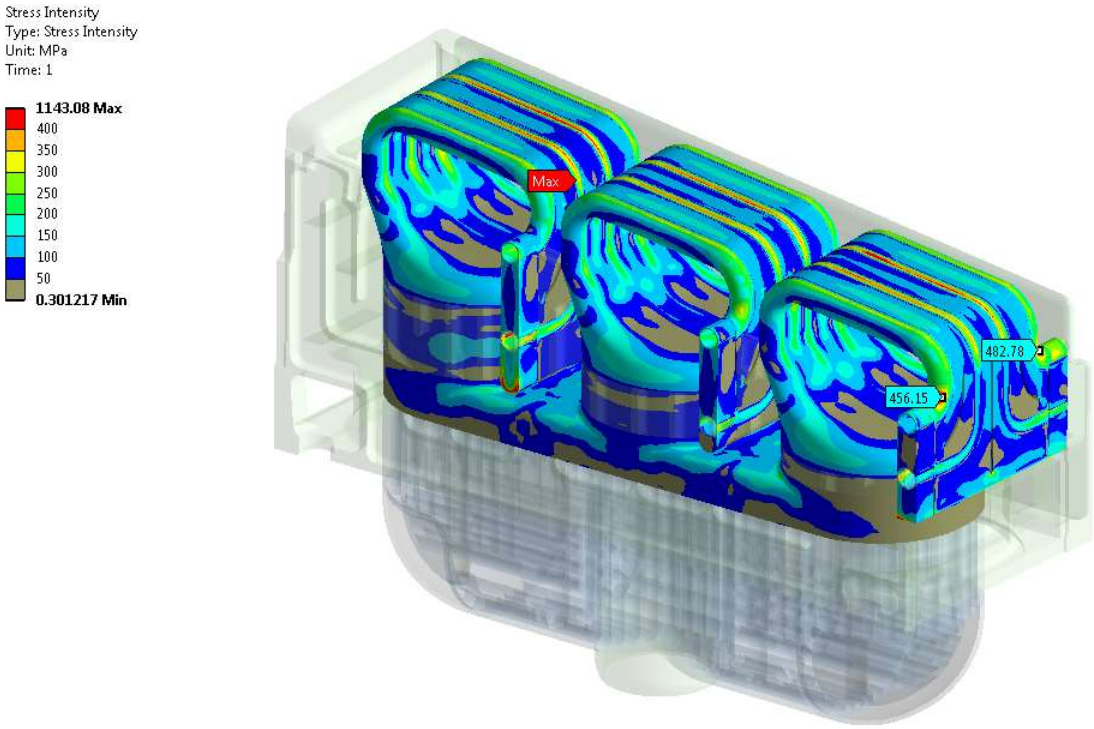


**Figure 12:** Stress intensity in the frontal sections of the ICH antenna - PDR design

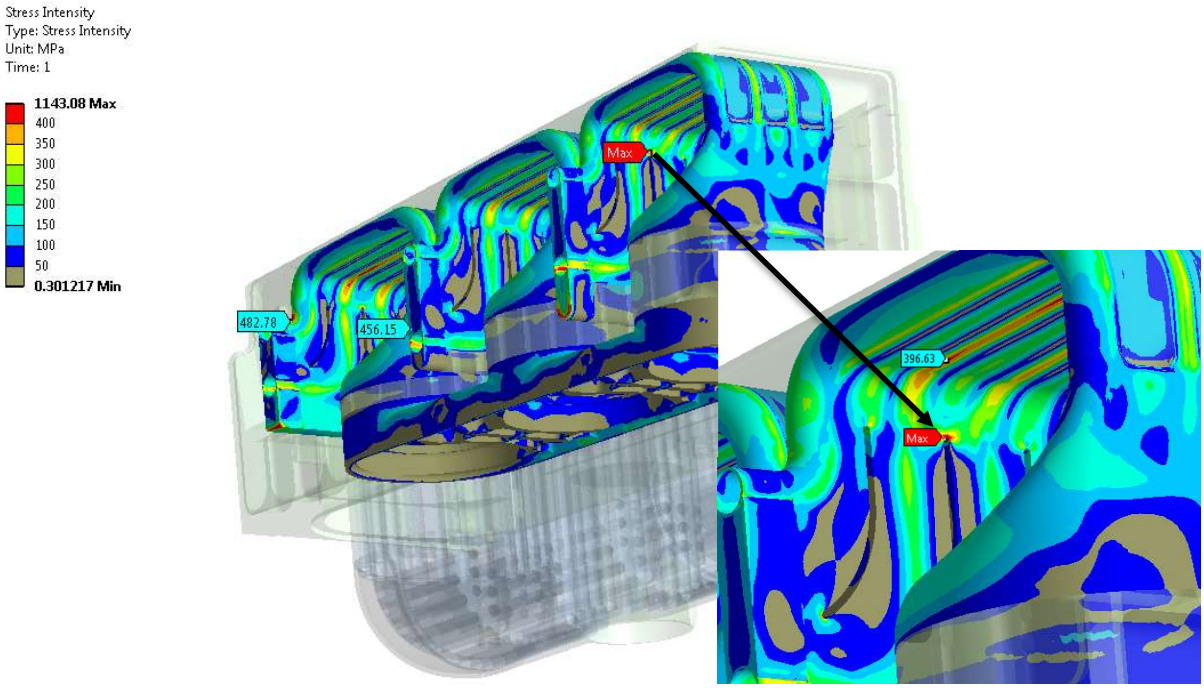


**Figure 13:** Area of maximum stress intensity in the straps of the ICH antenna - PDR design

Cooling channels persistently exhibit areas where the stress intensity reaches 450 MPa. In particular, these high stress areas are associated with the channel bends where thermal loading is also exceptionally high (Fig. 9). For comparison, Figs. 14 and 15 show the stress intensities (Tresca) for the proposed v12a design.

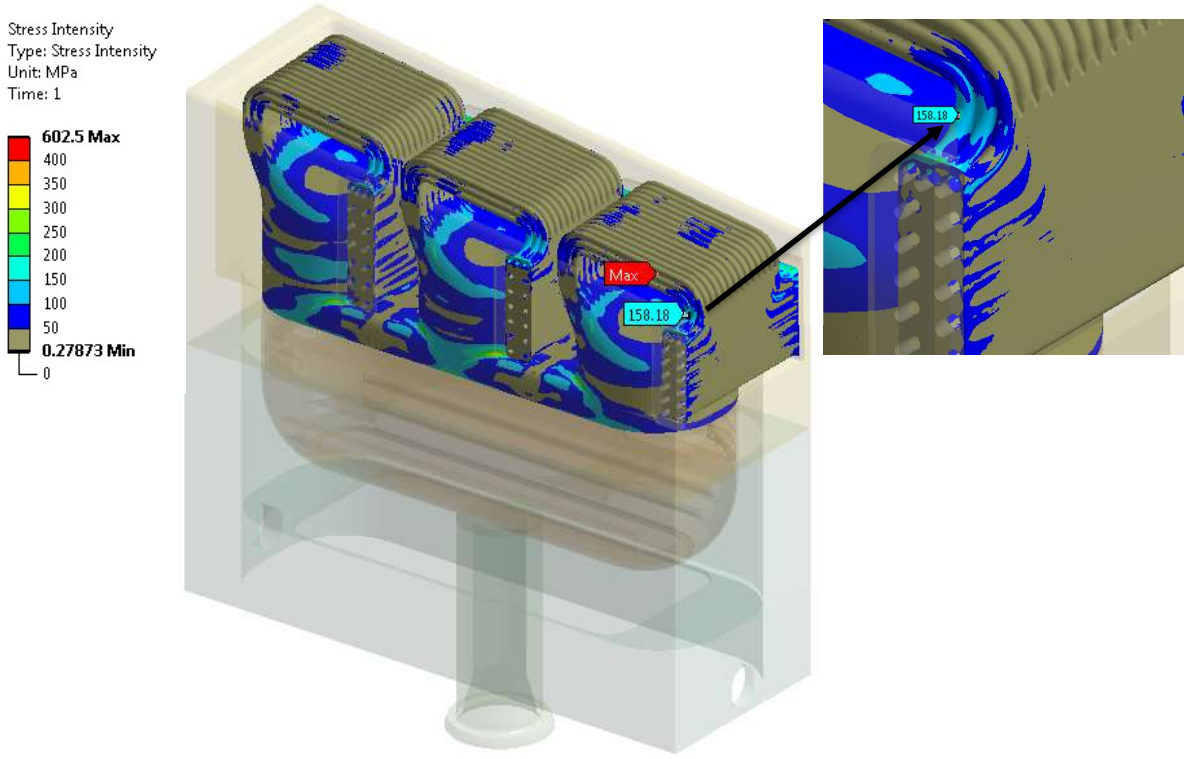


**Figure 14:** Stress intensity in the frontal sections of the ICH antenna - proposed v12a design

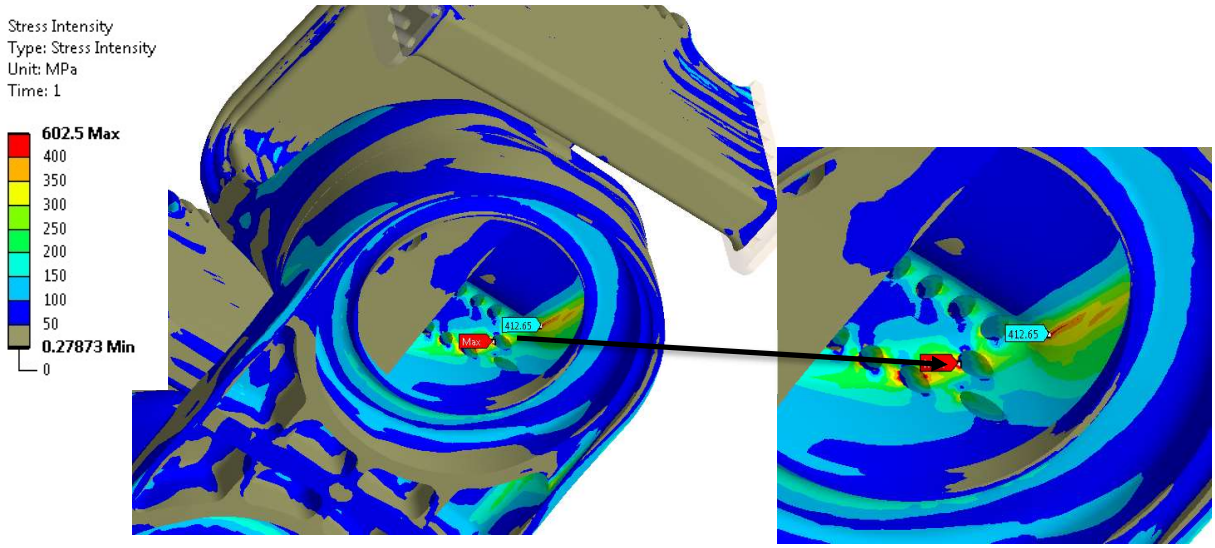


**Figure 15:** Area of maximum stress intensity in the straps of the ICH antenna - proposed v12a design

In general, the stress intensities are much lower than in the PDR design. The bends of the cooling channels no longer exhibit high stress values. Figure 14 shows that the local maximum in the bends does not exceed 160 MPa, which is well within the allowable stress limits for Inconel 625.

Elsewhere in the proposed v12a design, the highest stresses appear in the strap transition region (Fig. 15). The maximum value of 602 MPa is associated with a local stress concentration that may be reduced without any loss of the strap functionality. Nevertheless, the nearby wall area still exhibits stress intensity in excess of 400 MPa, which requires closer examination.

Stress linearisation was conducted and the following SDC-IC design rules [6] were used to demonstrate structural design compliance:

- Primary membrane and bending stress (immediate plastic collapse and plastic instability):

$$\overline{P_m} \leq S_m(T_m) \tag{4}$$

$$\overline{P_L + P_b} \leq K_{eff} S_m(T_m) \quad \text{where } K_{eff} = 1.5 \text{ or } 1.27 \text{ for a rectangular or pipe profile} \tag{5}$$

- Local primary membrane (immediate plastic collapse and plastic instability)

$$\overline{P_L} \leq min\left[1.5S_m(T_m), S_{y,min}(T_m)\right] \tag{6}$$

- Primary and secondary membrane stress (immediate plastic flow localisation)

$$\overline{P_L + Q_L} \leq S_e(T_m) \tag{7}$$

- Progressive deformation or ratcheting ($3S_m$ rule)

$$max(\overline{P_L + P_b}) + \Delta[\bar{P} + \bar{Q}]_{max} \leq 3S_m \tag{8}$$

  which excludes local peak stress ($F$) arising from geometrical discontinues. Additional information on the application of the design rule can be found in [9].

- Time-independent fatigue (see Table 3):

$$\Delta\sigma \leq S_a \quad [7] \tag{9}$$

  where $\Delta\sigma$ is the maximum stress range during the load cycle.

Table 4 summarises the calculated maximum stress levels in the straps for the NOC load case, and their compliance with the SDC-IC design rules. For all examined criteria, the calculated stresses are significantly lower than the design code limits thus demonstrating suitability of the proposed v12a design.

**Table 4:** Maximum stress intensities and SDC-IC code compliance for the frontal sections of the ICH antenna (NOC load case)

| Immediate plastic collapse and plastic instability | | | |
|---|---|---|---|
| | Limit | Reserve | |
| $\overline{P_m}$ = 64 MPa | 258 MPa | 4.0 | passes |
| $\overline{P_L + P_b}$ = 172 MPa | 387 MPa | 2.3 | passes |

| Immediate plastic flow localisation | | | |
|---|---|---|---|
| | Limit | Reserve | |
| $\overline{P_L + Q_L}$ = 144 MPa | 253 MPa | 1.8 | passes |

| Progressive deformation or ratcheting | | | |
|---|---|---|---|
| | Limit | Reserve | |
| $max(\overline{P_L + P_b}) + \Delta\bar{Q}_{max}$ = 324 MPa | 774 MPa | 2.4 | passes |

| Time-independent fatigue | | | |
|---|---|---|---|
| | Limit | Reserve | |
| $\Delta\sigma$ = 203 MPa | 640 MPa | 3.2 | passes |

## Conclusions

In the framework of the completed project a new design of ICH antenna straps was developed. Convective cooling was enhanced whilst maintaining the coolant mass flow rate. Also, thermal resistance between the load surfaces and the coolant flow was reduced by minimising the wall thickness of cooling channels.

Monte Carlo simulations of radiative heat transfer allowed for a more accurate definition of the thermal loading related to plasma and charge exchange. In addition, copper and stainless steel 316L(N) were replaced with Inconel 625, which exhibits much higher allowable stress limits.

Thermal and structural FE analyses were conducted for the normal operating conditions (NOC) to demonstrate compliance of the proposed v12a strap design with the SDC-IC design criteria. The presented results show that the calculated maximum stress levels satisfy the design stress limits for immediate plastic collapse and plastic instability, immediate plastic flow localisation, progressive deformation or ratcheting, and time-independent fatigue.

The presented design effort is limited to the ICH straps and the normal operating conditions (NOC). Further development of the 4-port junction and the strap housing design is still on-going. However, the design of these sections is predominantly defined by forces induced by EM disruption events and not by thermal loading that is characteristic for normal operating conditions.

## References


1. J. Wise, C02 - ICRH Antenna Straps and 4-Port Junction PDR Structural Analysis Report, ITER_D_GFTTSK_V1.0, 2013.

2. A. Lafuente, M. Fursdon and M. Shannon, Thermo-Structural Optimization of the ITER ICRH Four Port Junction and Straps against In-Vessel Design Criteria, Fusion Engineering and Design, Vol. 89, Iss. 7–8, Oct. 2014, pp 1784-1789.

3. N. Dalton and M. Fursdon, Thermo-Structural Evaluation of the ITER ICRH 4PJ and Straps against SDC-IC, CIA/D15-C2, Issue 3, ITER_D_9QVXS8 v1.1, 2012.

4. J. M. Pancheco Cansino, Load Specification for the ICH & CD Antenna, F4E IDM 2AC2DQ / 1.0, 2017.

5. A. Turner, ICRH 2012 Neutronics Model Update and Results, Report CIA/T/045, 2013.

6. ITER, In-vessel Components, SDC-IC, v. 3.0, G 74 MA 8 01-05-28 W 0.2, 2012.

7. A. Horvat, Structural Analysis Report for the Optimised Design of ICH Antenna Straps and -4-Port Junction, F4E_D_ 2C2U9V, Issue 2, 2018.

8. M. Webb, N. Mantel, R. Bamber, M. Fursdon, A. Horvat and F. Durodié, ICRH Antenna Final Report for Task Order 2, F4E_D_2BFMBT, Issue 1.1, 2018.

9. RCC-MRx Design and Construction Rules for Mechanical Components in Nuclear Installations, 2012, Section III - Tome I - Subsection B, RB 3261.1118.